Contents lists available at ScienceDirect

Applied Clay Science

journal homepage: http://ees.elsevier.com

Research Paper

Iron speciation in Opalinus clay minerals

N. Finck *

Institute for Nuclear Waste Disposal (INE), Karlsruhe Institute of Technology (KIT), P.O. Box 3640, Karlsruhe D-76021, Germany

ARTICLE INFO

Keywords
Opalinus clay
Illite
Iron
XRD
FTIR
Polarized XAS

ABSTRACT

Clay formations are under considerations in various countries to host a deep geological repository for high-level nuclear waste owing to beneficial physicochemical properties. These properties can, however, be influenced by the chemical form of structural Fe. The goal of this study was to obtain information on speciation of Fe associated with the clay fraction separated from the Opalinus clay rock, one of the clay formations at an advanced stage of repository planning. The clay rock was purified and the clay fraction was separated. Analyses by X-ray powder diffraction evidenced the presence of 1:1 (kaolinite) and 2:1 layer minerals (e.g., illite and possibly illite/smectite mixed layers), no other phase in significant amounts could be detected. Infrared spectroscopy corroborated the presence of both 1:1 and 2:1 layer minerals, and the absence of $Fe^{3+}{}_2$-OH bending in the spectrum ruled out extensive Fe clustering and hinted at a rather homogeneous distribution within the structure. Information on Fe speciation was obtained by X-ray absorption spectroscopy (XAS) at the *K*-edge. To reduce uncertainties on structural parameters, overlapping contributions from in-plane and out-of-plane shells were filtered by recording polarized XAS data. The position of the pre-edge feature indicated the prevalence of Fe^{3+}, while the intensity and splitting were typical of Fe located at octahedral site. The pre-edge of the reference kaolinite differed from that of the Opalinus clay sample, excluding the prevalence of Fe within that 1:1 layer mineral. Data thus suggested the prevalence of Fe^{3+} within the octahedral sheet of 2:1 layers. Polarized XANES and EXAFS exhibited significant angular dependencies hinting at the presence of various neighboring shells with specific orientations. The first O shell located at 2.03 Å contains about six O atoms oriented in-plane. At higher distances, three in-plane Al/Mg and Fe and about four out-of-plane Si atoms were detected at ~3.05 Å and 3.23 Å, respectively, suggesting that Fe is located in a dioctahedral octahedral sheet of 2:1 layers. The presence of significant amounts of Fe in the tetrahedral sheet was excluded. Combining results from XAS with that from chemical analysis enabled to estimate first the structural formula of the 2:1 layer fraction and subsequently the proportions of 1:1 and 2:1 layer minerals within the purified clay fraction of the Opalinus rock. The estimated proportions of 1:1 and 2:1 layer minerals were in reasonable agreement with that of the whole Opalinus rock.

1. Introduction

The final disposal of high-level nuclear waste (HLW) in deep geologic formations with the aim to isolate it from the biosphere is under investigation in various countries. In deep geological repositories (DGR), HLW is planned to be surrounded by a series of barriers, each having a capacity to prevent or lower the release of radionuclides to the environment (e.g., Ewing et al., 2016). Countries such as Belgium, France and Switzerland are at an advanced stage in their investigations on the possibility to select clay rock to host such a repository (e.g., ANDRA 2005; NAGRA, 2002). Clay rocks mainly consist of clay minerals, with additional phases such as other silicates (quartz, feldspar), carbonates (calcite, siderite) and minor amounts of pyrite (Grambow, 2016). Furthermore, bentonite, which is mostly made of highly reactive smectite (Christidis and Huff, 2009), may be used as backfill material in such a repository. Choosing to dispose of HLW in clay rock is motivated by the availability of an appropriate geologic formation, and because clay minerals have beneficial physicochemical properties, such as swelling, low hydraulic conductivity and high retention capacity (e.g., Grambow, 2016). These properties depend on the crystallochemistry of these minerals, and thus providing detailed information can help improving the understanding of the reactivity of the specific host rock.

Clay minerals belong to the phyllosilicate group and their crystal structure is made of octahedral and tetrahedral sheets (Meunier,

* Corresponding author.
E-mail address: nicolas.finck@kit.edu (N. Finck)

https://doi.org/10.1016/j.clay.2020.105679
Received 27 January 2020; Received in revised form 12 May 2020; Accepted 15 May 2020
Available online xxx
0169-1317/

2005). In 1:1 layers, one tetrahedral sheet binds one octahedral sheet (e.g., kaolinite or serpentine). In 2:1 layers, one octahedral sheet is sandwiched between two tetrahedral sheets and the layer charge originating from cationic substitution within the lattice is balanced by interlayer cations (e.g., smectite, illite or mica). Finally, in 2:1:1 layers (e.g., chlorite) the interlayer of 2:1 stacks is made of an octahedral sheet. Clay minerals exhibit a great diversity in their composition because of their large compositional ranges of solid solution and their ability to form polyphased crystals by interstratification (Meunier, 2005). Octahedral sites of clay minerals are commonly filled by Al^{3+}, Mg^{2+}, Fe^{2+} or Fe^{3+}. Tetrahedral sites are smaller and commonly filled by Si^{4+} atoms and can be substituted by Al^{3+}, more rarely by Fe^{3+}, whereas Fe^{2+} is less likely to fit tetrahedral sites because of its large size and possibly because of its difference in charge with Si^{4+}. This great flexibility of structural sites filling patterns can result in various locations and amounts of layer charge, which may affect the reactivity of clay minerals. For example, the location and amount of cationic (e.g., Vinci et al., 2020) and anionic substitutions (Dazas et al., 2015) in smectites affect their hydration properties and thus the transfer and fate of contaminants in surficial environments where these minerals are present.

The physicochemical properties of clay rock depend on the nature of clay particles present in the mineral assemblage. For example, smectites and illite are ubiquitous in clay rocks and in sedimentary deposits, and their content varies with the geochemical conditions (e.g., temperature and pressure) of the environment where they are present (e.g., Meunier and Velde, 1989; Ferrage et al., 2011). Indeed, an increase in temperature and pressure favors the transition from the expandable layers smectite to the non expandable layers illite in a reaction called smectite illitization (Lanson et al., 2009; Ferrage et al., 2011), and which proceeds through an evolution of the layer charge driven by atomic substitutions (Berthonneau et al., 2017). Interestingly, such geochemical conditions are also expected to develop after closure and water resaturation of a DGR for HLW. Under such anoxic, elevated temperature and water-saturated conditions, steel canisters containing HLW will corrode, resulting in the formation of Fe^{2+} and in the production of hydrogen. Upon contact with Fe^{2+} clay minerals are expected to be destabilized, followed by the formation of Fe-rich 1:1 layered silicates (e.g., Schlegel et al., 2014; Mosser Ruck et al., 2020). Interestingly, earlier studies suggested that clay destabilization actually starts with the release of protons bound to Fe^{3+} from the clay octahedral sheet and that no reaction is observed when structural Fe^{3+} is absent (Lantenois et al., 2005). Besides, the production of hydrogen upon steel corrosion will lead to an increase in pressure and to the evolution of reducing conditions, which may also favor the reduction of structural ferric ion to ferrous ion. Furthermore, the presence or existence of microorganisms in repository-type sites, residing in the host rock and associated groundwater, has been reported in several studies (Mullican et al., 2009), and microbial activity can also lead to the reduction of structural iron in clay minerals (Kim et al., 2004; Stucki and Kostka, 2006; Li et al., 2019). Consequently, the composition of clay minerals of a DGR, and thus its physicochemical properties, may evolve with time and to some extent depend on the content and speciation of structural iron.

A modification of the oxidation state of structural iron in clay minerals can have various impacts over the course of the geochemical evolution of the repository system. For example, the reduction of structural iron has been shown to modify the physicochemical properties of the clay rock and the bentonite backfill (Stucki and Kostka, 2006; Stucki, 2011; Liu et al., 2012), which in turn will affect the performance of the barrier. Similarly, a reduction in Fe oxidation state will modify the retention properties towards radionuclides (Xia et al., 2005; Bishop et al., 2011; Joe-Wong et al., 2017) mobilized upon HLW matrix alteration. Because the extent of structural Fe^{3+} reduction depends on the layer charge, the charge location and on the Fe content (Gorski et al., 2013), detailed studies on specific clay minerals are needed to improve the safety case of a repository.

Numerous studies performed in the laboratory reported the reduction of structural Fe in clay minerals by use of chemicals (e.g., Stucki et al., 1984; Komadel et al., 2006; Ilgen et al., 2019) or by application of electrochemical methods (e.g., Gorski et al., 2012). Detailed analysis of reduced clay minerals revealed that the reduction of structural Fe^{3+} is accompanied by a dehydroxylation of the octahedral sheet and induces the migration of Fe from *cis* to *trans* octahedral sites, resulting in the formation of defects separated from small trioctahedral domains (Manceau et al., 2000a; Neumann et al., 2011). In Fe-rich smectites (nontronites) the formed defects are enclosed within these trioctahedral domains (Neumann, 2011), and the re-oxidation of reduced Fe is only partially reversible.

In most investigations reporting structural characterizations of the chemical form of structural Fe within clay minerals (e.g., Manceau et al., 2000a, 2000b; Vantelon et al., 2003; Finck et al., 2015, 2019), information was obtained by applying complementary spectroscopic techniques such as infrared and X-ray absorption spectroscopy. Infrared spectroscopy probes the whole structure, especially the octahedral sheet because all OH-sharing cation pairs contribute to the spectrum and because it has no chemical selectivity (Gates, 2008). In contrast, X-ray absorption spectroscopy (XAS) is element specific and provides information on the average number of neighboring atoms for Fe located at all possible positions. Unfortunately, the nearest octahedral and tetrahedral cationic shells of octahedral Fe in clay minerals are located at ~3.04–3.10 Å and at ~3.25–3.30 Å, respectively, resulting in overlap of EXAFS contributions, thereby reducing the precision of quantitative analysis of EXAFS spectra. However, this limitation can be overcome by performing polarized EXAFS measurements on clay minerals prepared as highly textured samples. The contribution of cations from the tetrahedral sheet can be minimized by orienting the clay layer plane parallel to the electric field of the incoming X-ray beam (angle $\alpha = 0°$), whereas the contribution of cations from the octahedral sheet is minimized in the perpendicular orientation ($\alpha = 90°$). In a polarized XAS experiment, the actual coordination number of neighboring atomic shells is obtained at $\alpha = 35°$, and powder and polarized XAS are identical. A deviation from this value may result in overestimation or underestimation of the number of neighboring atoms. Note that powder and polarized XAS are also identical when the angle between the vector connecting the absorber to the backscatterer and the layer normal equals 54.7° regardless of α. The successful application of polarized XAS in separating contributions of next-nearest octahedral and tetrahedral cationic shells is amply documented in the literature (Manceau, 1990; Manceau et al., 1998, 2000a, 2000b; Schlegel et al., 1999; Finck et al., 2015, 2017, 2019). Finally, information on either statistical or preferential distribution in clay minerals can be provided by comparing the number of detected cationic neighbors with values expected from structural formula or from weight content (e.g, Finck et al., 2019).

The above-mentioned studies typically focused on well-defined, i.e., monomineral materials and hardly any work on clay minerals of rocks currently under consideration in various countries for hosting a deep repository (e.g., Boom Clay, Callovo-Oxfordian, Opalinus) has been reported. For example, the Opalinus clay rock is an assemblage mostly made of clay minerals with significant amounts of admixed carbonates and other silicates (quartz, feldspar), and low amounts of pyrite (NAGRA, 2002b; Bath and Pearson, 2003). The goal of this study was to provide information on the crystal chemistry of structural Fe in the clay mineral fraction isolated from the Opalinus clay rock. Clay mineral phases present in the sample were identified and characterized by various techniques in the laboratory. The sample was prepared as self-supporting film to obtain information on Fe speciation by polarized X-ray

absorption spectroscopy (XAS) at the *K*-edge. Results from quantitative EXAFS analysis combined with the chemical analysis of the sample were used to estimate the structural formula of the mineral phase hosting Fe, and to estimate the proportions of the mineral phases present in the isolated clay fraction.

2. Materials and methods

The Opalinus clay rock used in this study was sampled in 2007 (batch BLT-14 (Nussbaum et al., 2008)) at Mont Terri (Switzerland) by BGR (Bundesanstalt für Geowissenschaften und Rohstoffe, Hannover, Germany). Opalinus clay was deposited about 180 million years ago in a rather shallow marine environment of the Jurassic sea and is presently found throughout northern Switzerland (Bath and Gautschi, 2003). The Mont Terri Rock Laboratory is situated in a 3900 m long motorway tunnel in the Jura mountains of northern Switzerland, in this area the Opalinus Clay formation has a vertical thickness of about 160 m. The borehole was drilled in sandy facies, which typically contain various clay minerals, such as illite, illite/smectite, chlorite and kaolinite, amounting to 45–70% of the whole rock (Bath and Pearson, 2003). The rock also contains significant amounts of quartz (16–32%) and carbonate phases, mostly calcite (7–17%), along with dolomite/ankerite and siderite. Finally, lower amounts of feldspar, pyrite and organic carbon are present as well in the rock. After drilling, the rock was kept under anoxic conditions until use in this study. All subsequent steps (purification, fractionation and analyses) were performed under ambient conditions. The powdered sample was suspended in water, converted to Na form by repeatedly washing with 1 mol/L NaCl, treated shortly with HCl at pH 3–4 in 1 M NaCl and brought back to neutral conditions by washing with 1 M NaCl. No additional chemical treatment was applied to avoid altering the structure at the platelet edges or the chemical state of Fe by using e.g. dithionite which is typically used to remove admixed Fe (hydr)oxides (e.g., Moore and Reynolds Jr., 1997) and which can as well reduce structural Fe (e.g., Stucki et al., 2002 and references therein). In order to remove fine-grained accessory mineral phases successive sedimentation and centrifugation steps were applied to separate the fraction <0.1 μm which was the target product (Finck et al., 2019).

The mineralogical composition was determined by X-ray powder diffraction (XRPD) using a D8 Advance (Bruker) diffractometer (Cu Kα radiation, LynxEye XE-T detector). Complementary information was obtained by Fourier transform infrared (FTIR) spectroscopy (IFS55 Bruker Optics, ATR accessory, DTGS detector) under ambient conditions. For polarized XAS measurements, the Opalinus clay sample was prepared as self-supporting film by slow vacuum filtration of the suspension on a mixed cellulose esters filter of 0.025 μm pore size (Merck Millipore). This protocol readily provided a highly textured sample with *a* and *b* axes randomly oriented in the film plane (Manceau et al., 1998). The high orientation was checked by recording scanning electron micrographs using an environmental scanning electron microscope (Quanta 650 FEG, FEI), and information on chemical composition was provided by energy-dispersive X-ray spectroscopy (EDX).

Fe *K*-edge X-ray absorption spectroscopy (XAS) data were recorded at the BM30B beamline (Proux et al., 2005) at the European Synchrotron Radiation Facility (ESRF, Grenoble, France) with a storage ring energy of 6 GeV. The incoming X-ray beam was monochromatized using a pair of Si⟨220⟩ crystals and the energy was calibrated by assigning the first inflection point of the *K*-edge XANES recorded from a Fe foil to 7112 eV. For polarized XAS measurements, the self-supporting film was mounted on a goniometer and spectra were recorded in transmission mode considering several angles between the electric field of the X-ray beam and the film plane (α = 10, 35, 55 and 80°). The experimental uncertainty on α is estimated to ±1°. Powder X-ray absorption spectra were also recorded for several reference compounds: raw kaolinite (KGa1b), the purified <0.1 μm fraction of a dioctahedral smectite (montmorillonite SWy-2), the purified <0.1 μm fraction of a trioctahedral smectite (hectorite SHCa-1) and $FePO_4$ (rodolicoite, reference compound for tetrahedral ferric ion $^{[4]}Fe^{3+}$).

XAS data were analyzed following standard procedures using Athena and Artemis interfaces to the Ifeffit software (Ravel and Newville, 2005). EXAFS spectra were extracted from the raw data and Fourier transforms (FTs) were obtained from the $k^3 \times \chi(k)$ functions. Data were fit in *R*-space using phase and amplitude functions calculated with feff6 (Ankudinov et al., 1998), and the amplitude reduction factor set to 0.75, a value well suited to properly fit the data of goethite (α-FeOOH) (data not shown). Theoretical paths were generated using the published structure of 2:1 layer montmorillonite (Tsipursky and Drits, 1984), with the absorber (Fe) located at octahedral position. Because differences in backscattering amplitude between Mg, Al and Si are very limited, data were modeled considering only Al as octahedral neighbor and Si as tetrahedral neighbor. The presence of Fe at octahedral and at tetrahedral position was tested. Polarized XAS data were fit simultaneously at all angles using a single value of shift in ionization energy (ΔE_0), and for a given atomic shell a common bond length and mean squared displacement (Debye-Waller term) (Schlegel and Manceau, 2013; Finck et al., 2015, 2017, 2019). Furthermore, the Fe/Al atomic ratio was kept equal at all angles. At all angles the Fourier transform range was 4.1–11.0 $Å^{-1}$ and the fit range was 1.2–3.4 Å. Fits to the pre-edge features were obtained using the OriginPro 2017 software as described earlier (Finck et al., 2015).

3. Results and discussion

3.1. X-ray powder diffraction, infrared spectroscopy and electron microscopy

The X-ray powder diffraction pattern identified the presence of kaolinite and illite in the purified clay mineral fraction of the rock (Fig. 1, top). The broad reflection at 8–9° 2θ may also suggest the possible presence of mixed layer minerals (illite/smectite) (Meunier and Velde, 2004). The absence of sample swelling upon exposure to ethylene glycol (data not shown) excludes the presence of pure smectites, and no significant amount of other crystalline phase could be detected. Earlier studies on the original rock (i.e. not purified and not fractionated) indicated the presence of additional phases such as silicates and carbonates (NAGRA, 2002b; Bath and Pearson, 2003). In this study such admixed phases were removed by purification and fractionation of the clay rock.

The infrared spectrum (Fig. 1, middle) contains bands at 3700, 3670, 3648 and 3621 cm^{-1} corresponding to hydroxyl stretching and the band at 910 cm^{-1} to hydroxyl deformation of kaolinite (Madejova and Komadel, 2001). The band at 457 cm^{-1} is attributed Si-O-Si deformation and bands at 752 and 687 cm^{-1} to Si-O perpendicular (Madejova and Komadel, 2001). The presence of illite in the sample is evidenced by bands sometimes overlapping with that characterizing kaolinite, such as -OH stretching at 3623 cm^{-1}, and Al_2-OH and AlMg-OH bending at 910 and 830 cm^{-1}, respectively (Inoue and Watanabe, 1989). The band at 517 cm^{-1} can be attributed to Al-O-Si deformation and bands at 752 and 687 cm^{-1} to in-plane vibration of Al-O-Si in the tetrahedral sheet and to Si-O-Si stretching, respectively (Madejova and Komadel, 2001). Note that the presence of the band at 752 cm^{-1} hints at substantial Al for Si substitution in the tetrahedral sheet. The weak band near 800 cm^{-1} can be attributed to Fe^{3+}Mg-OH bending (e.g. Gates, 2008). The intense band at 986 cm^{-1} is typical of Si-O stretching of clay minerals, with the shoulder at 1097 cm^{-1} attributed to Si-O stretching in the longitudinal mode (Madejova and Komadel, 2001). The absence of Mg_3-OH (near 650 cm^{-1}) and $Fe^{3+}{}_2$-OH (near 820 cm^{-1}) bending bands in the FTIR spectrum (Gates, 2008; Finck et al., 2019) rule out extensive Mg and Fe clustering. Furthermore, the

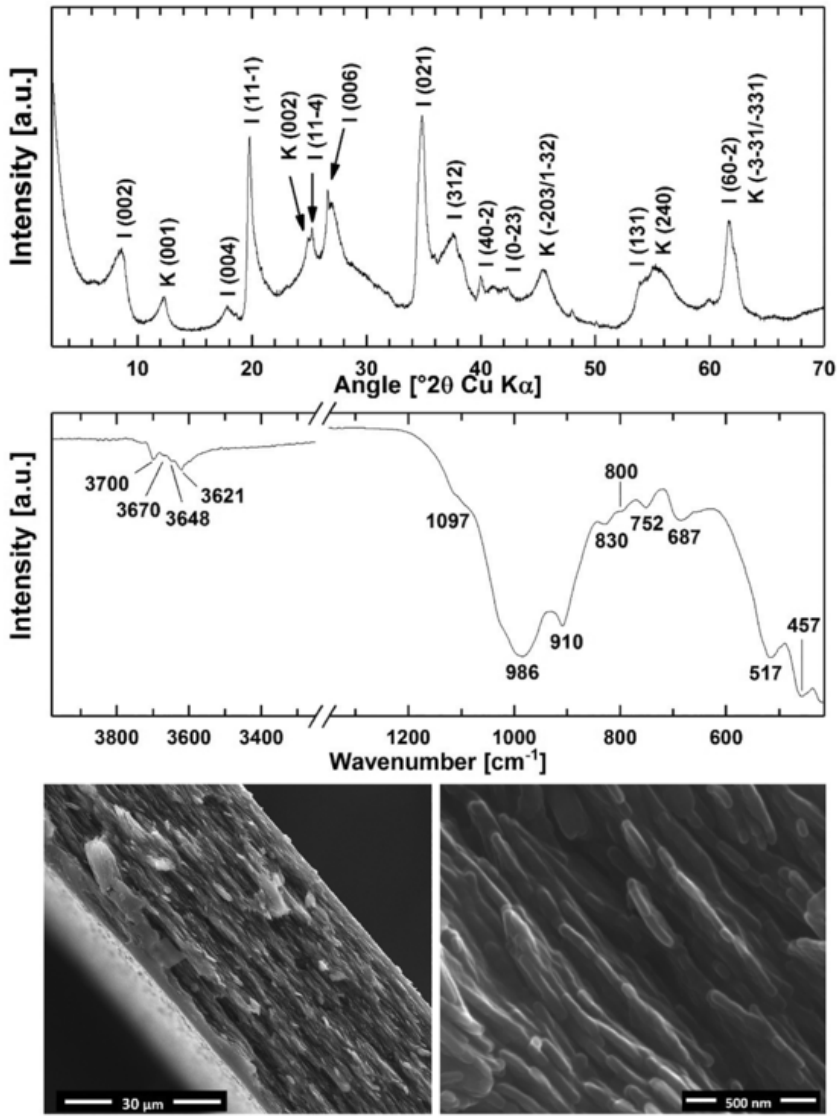

Fig. 1. X-ray powder diffractogram (up), Fourier transform infrared spectrum (middle) and scanning electron micrographs of the investigated purified and fractioned Opalinus clay sample (bottom). On the diffractogram, I stands for illite (2*M* polytype), K for kaolinite and numbers in parentheses indicate *hkl* planes.

absence of Fe^{3+}Al-OH bending (near 870 cm^{-1}) rules out the presence of significant amounts of Al-Fe pairs, whereas the presence of the Fe^{3+}Mg-OH bending near 800 cm^{-1} suggests the presence of octahedral Mg-Fe pairs. Infrared spectroscopy thus corroborates the presence of 1:1 and 2:1 layer minerals in the sample, with a low but significant Al for Si substitution in the tetrahedral sheet and with a preferential formation of Mg-Fe^{3+} pairs in the octahedral sheet. No other mineral phase could be detected in the sample.

Electron micrographs (Fig. 1, bottom) show that the self-supporting sample has a thickness of ~40 µm with clay platelets well oriented within the film plane, and thus that it is well suited for performing angular-dependent XAS experiments (Manceau and Schlegel, 2001). SEM-EDX provides information on chemical composition of the sample: 51.2 wt% O, 0.7 wt% Na, 1.6 wt% Mg, 14.0 wt% Al, 24.1 wt% Si, 4.3 wt% K and 4.1 wt% Fe. Results reveal a moderate Fe content and significant Al and Si contents. The substantial Al and low Mg contents are in line with dioctahedral frameworks (kaolinite and illite). Furthermore, the low Na and substantial K content also agree with the presence of illite and thus the absence of swelling upon exposure to ethylene glycol. No iron-containing phase other than clay minerals could be detected in the sample and FTIR spectroscopy rules out compelling Fe clustering, implying that iron can be used as local probe to gain information at the atomic scale by application of XAS.

3.2. X-ray absorption spectroscopy

Pre-edge spectroscopy. Pre-edge spectra of first-row transition metals arise predominantly from $1s \rightarrow 3d$ transitions (Waychunas et al., 1983; Westre et al., 1997). When Fe is in a centrosymmetric environment (e.g., O_h symmetry), these transitions are electric dipole forbidden. No pre-edge should thus be observed for octahedrally coordinated Fe such as in clay minerals but low intensity pre-edge features are still experimentally observed (e.g., Manceau et al., 2000a, 2000b; Finck et al., 2015, 2019) because of local symmetry. Indeed, the presence of vacancies in dioctahedral frameworks alters the geometry of the octahedra, and thereby the local symmetry around octahedral cations, whereas distortions are more limited in trioctahedral sheets (Meunier, 2005). Consequently, a portion of formerly forbidden transitions becomes allowed through introduction of a trigonal symmetry at octahedral site, resulting in an increase in pre-edge intensity. In a non-centrosymmetric environment the metal 4*p* mixing into the 3*d* orbitals provides some electric dipole allowed $1s \rightarrow 4p$ character to the transition

resulting in the observation of features of substantial intensity for e.g., fourfold coordinated Fe (e.g., T_d symmetry (Manceau et al., 2000b; Finck et al., 2019)).

The pre-edge of montmorillonite and hectorite is split into two components (t_{2g}- and e_g-like components) and is of lower intensity than that of $FePO_4$, but in all three compounds the pre-edge has similar energy position of the centroid (Fig. 2, Table 1). These samples contain only ferric ion, with sixfold coordination in the smectites and fourfold coordination in $FePO_4$ (Finck et al., 2015; Cipriani et al., 1997). The pre-edge of the kaolinite differs from that of the smectites and three components were used to fit experimental data. Two of these components are located at energy positions typical of octahedral ferric ion, whereas the third component is at lower energy, hinting at the possible simultaneous presence of ferric and ferrous ion in the kaolinite.

The pre-edge of Opalinus at α = 35° (at this angle powder and polarized XAS data are identical) differs from that of $FePO_4$ and from that of kaolinite. In contrast, it is comparable to that of the montmorillonite, with similar energy position, intensity, energy separation of the components and ratio of low energy component integral to high energy component integral ($R_{I1/I2}$, Fig. 2, Table 1). Though the Opalinus clay sample is a mixture of 1:1 and 2:1 layers, pre-edge spectra indicate the prevalence of ferric ion at octahedral sites within dioctahedral 2:1 layers. Polarized pre-edge features exhibit significant angular dependence (Fig. 3, Table 1), hinting at an anisotropic environment. Interestingly, $R_{I1/I2}$ does not change monotonically with α, but increases from 10° to 35° and then decreases. This finding is consistent with reported studies

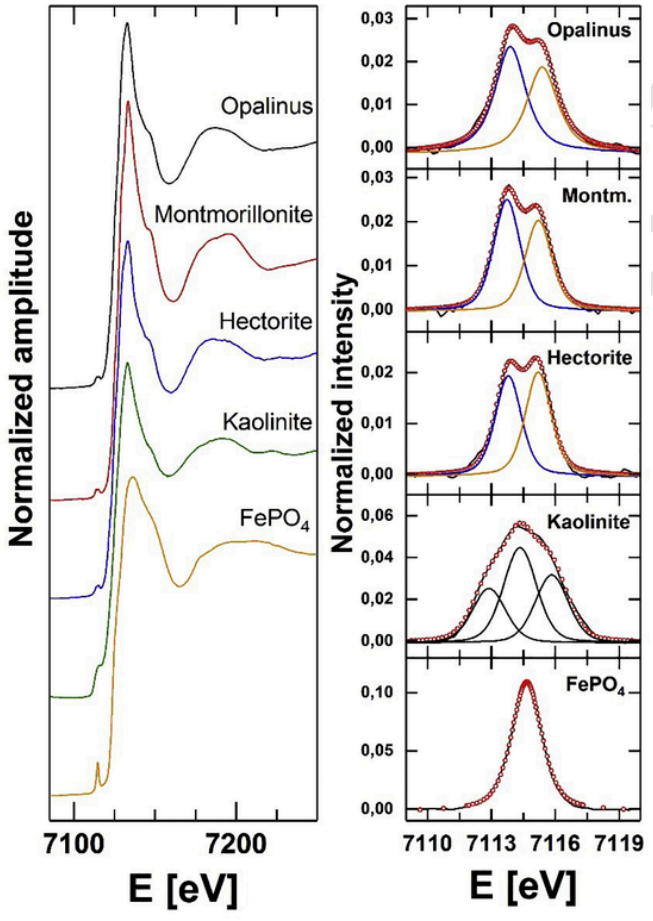

Fig. 2. Experimental XANES (left), and experimental and modeled (red dots) pre-edge features with individual components (right) of the purified and fractioned Opalinus clay sample (α = 35°) and other reference compounds (α = 35° for montmorillonite and hectorite). Fit results are presented in Table 1. (For interpretation of the references to colour in this figure legend, the reader is referred to the web version of this article.)

Table 1
Results of fits to the pre-edge features, data are shown in Figs. 2 and 3. Uncertainties on energies are estimated to ±0.1 eV and on integrals to ±10%. $R_{I1/I2}$ is the ratio of the low energy component integral to the high energy component integral.

Sample	α [°]	Pre-edge peak energy [eV]	Pre-edge peak integral	Energy separation [eV]	Integral ratio ($R_{I1/I2}$)
Purified and fractioned Opalinus clay sample	10	7113.82	0.061	1.57	0.80
		7115.39	0.076		
	35	7113.89	0.060	1.50	1.25
		7115.39	0.048		
	55	7113.84	0.071	1.60	1.09
		7115.44	0.065		
	80	7113.73	0.066	1.57	0.81
		7115.30	0.081		
Montmorillonite	35	7113.73	0.046	1.48	1.21
		7115.21	0.038		
Hectorite	35	7113.80	0.035	1.40	0.95
		7115.20	0.037		
Kaolinite	/	7112.88	0.056	/	/
		7114.34	0.099		
		7115.83	0.071		
$FePO_4$	/	7114.66	0.244	/	/

(Dyar et al., 2001; Finck et al., 2015) and may suggest that the transition is predominantly quadrupole (Hahn et al., 1982).

X-ray absorption near-edge structure (XANES). The powder XANES of the Opalinus clay sample bears similarities with that of both smectites, such as energy position and height of the edge crest, suggesting a chemical environment similar to that in these compounds rather than to that of the kaolinite (Fig. 3). This finding is in agreement with the inspection of the pre-edge. Dissimilarities with reported XANES of ferric saponite (Finck et al., 2019) further exclude the presence of tetrahedral iron. Polarized XANES (Fig. 3) exhibit significant angular dependencies and contain well-defined isosbestic points, indicating that Fe is located in an anisotropic environment with the presence of neighboring atomic shells of distinct orientations. This finding attests to the high degree of particles orientation within the film and rules out the presence of admixed Fe-containing phase, which would not exhibit any angular dependence. The decrease in XANES main absorption edge intensity for increasing α values hints at an in-plane orientation of neighboring atomic shells.

Extended X-ray absorption fine structure (EXAFS). Polarized EXAFS spectra exhibit significant angular dependencies (at e.g., 5.0, 5.5, 6.1 and 8.0 $Å^{-1}$), with variations in amplitude and position of oscillation maxima (Fig. 4). Accordingly, Fourier transforms (FTs) also exhibit significant angular dependencies: the amplitude of the peak at $R + \Delta R \sim 1.6$ Å decreases with increasing α values, whereas the more complex angular dependence of the contribution centered at ~2.8 Å suggests the presence of more than one shell (Manceau et al., 2000b; Finck et al., 2015, 2019). The observation of isosbsetic points further corroborates the high texture of the sample.

The FT peak at $R + \Delta R \sim 1.6$ Å corresponds to an O shell and best fit results yield an Fe-O interatomic distance of d(Fe-O) = 2.03(1) Å and a coordination number at α = 35° of N^{35}_O = 6.0(4) (Table 2, Fig. 4). Fit results match reported values of ferric ion at clay octahedral sites and rule out the presence of tetrahedral Fe (Manceau et al., 2000b; Vantelon et al., 2003; Finck et al., 2015, 2019). The amplitude of this FT peak decreases with increasing α, and the number of detected O atoms decreases from 6.2(4) at α = 10° to 5.1 at α = 80°. The orientation of this shell can be estimated using the relationship between the variation of N_O as a function of α and the angle (β_O) between the absorber-backscatterer pair and the normal to the film plane

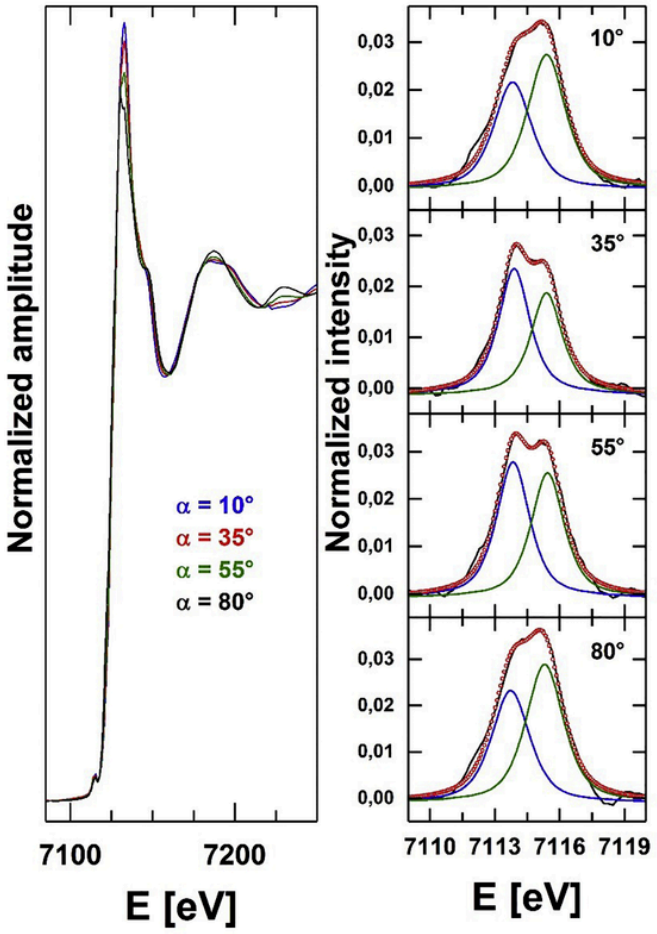

Fig. 3. Experimental XANES (left), and experimental and modeled (red dots) pre-edge features with individual components (right) of the purified and fractioned Opalinus clay sample at various angles α. Fit results are presented in Table 1. (For interpretation of the references to colour in this figure legend, the reader is referred to the web version of this article.)

(Schlegel et al., 1999). The calculated β_O of 57.4(1.5)° is comparable to reported value for montmorillonite (Finck et al., 2015) and in agreement with the octahedral flattening observed in most hydrous phyllosilicates (Güven, 1988). Besides, the observation of pre-edge features is a direct consequence of this deviation from the theoretical value of 54.7° for fully symmetric octahedra.

Higher distance contributions were modeled (Fig. 4, Table 2) considering Al, Fe and Si backscatterers located at d(Fe-Al) = 3.03(1) Å, d(Fe-Fe) = 3.06 Å and at d(Fe-Si) = 3.23 Å, respectively. These interatomic distances are typical of atomic shells surrounding octahedral Fe within clay minerals (e.g., Manceau et al., 1998, 2000a, 2000b; Vantelon et al., 2003; Finck et al., 2015, 2019). Fit results indicate a moderate contribution from neighboring Fe, with on average less than ¼ of neighboring octahedral sites occupied by Fe. Given the moderate Fe content of the sample (~4 wt% Fe), data rule out a preferential (e.g., clustering) distribution. The absence of preferential distribution would agree with reported findings (Finck et al., 2015, 2019) and with the absence of Fe^{3+}-OH bending band in the infrared spectrum. The number of detected Al (N_{Al}) and Fe (N_{Fe}) decrease with increasing α values while N_{Si} increases, suggesting predominantly in-plane orientation of Al and Fe (i.e., located in the octahedral sheet) and out-of-plane orientation of Si (i.e., located in the tetrahedral sheet).

In dioctahedral 1:1 and 2:1 layers, octahedral cations have three in-plane cationic neighbors but only two tetrahedral neighbors in the former structure and four in the latter. The number of neighboring cations can thus inform on the nature of the phase hosting Fe in the Opalinus clay sample. The number of neighboring octahedral cations at α = 35° is typical of a dioctahedral framework with $N^{35}_{Al} + N^{35}_{Fe} = 3$. The number of tetrahedral neighbors N^{35}_{Si} = 3.4(4) is slightly lower than the theoretical value of 4 in 2:1 layers, but equals reported values for montmorillonite (Finck et al., 2015). Assuming all Fe is located in 2:1 layers only, several explanations could possibly explain the deviation from the ideal value. First, the contribution from neighboring tetrahedral cations was modeled considering the presence of Si only whereas infrared spectroscopy data hint at substantial Si substitution by Al. Al and Si differ only by Z ± 1 meaning that differences in backscattering amplitude between these cations are limited, but very likely not completely negligible given the amount of tetrahedral Al. Second, the difference in atomic radii (Shannon, 1976) between these fourfold coordinated cations ($r(^{[4]}Al^{3+})$ = 0.39 Å; $r(^{[4]}Si^{4+})$ = 0.26 Å) is substantial, which may cause an increase in the dimension of the tetrahedral sheet and thus the size mismatch with the octahedral sheet. The size misfit is compensated by a rotation of octahedra around the layer normal, and the induced structural strain yields a broad distribution in Fe–(Si,Al) bond lengths (Manceau et al., 2000b) resulting in an underestimation of the number of tetrahedral cationic neighbors compared to the crystallographic value of 4. Consequently, experimental data suggest that only very low amounts of Fe might be located within the octahedral sheet of the 1:1 layer fraction of the Opalinus clay sample. This finding agrees with the reported low Fe content within kaolinite compared to e.g., smectites (e.g., Mermut and Cano, 2001).

3.3. Further information on the clay sample

The investigated purified and fractioned Opalinus clay sample is an assemblage made of 1:1 (i.e. kaolinite) and 2:1 layers (i.e. illite and possibly illite/smectite mixed layers), no other crystalline phase could be detected. Spectroscopic data further hint at the prevalence of octahedral ferric ion in a dioctahedral framework, predominantly in 2:1 layers. Because no extensive iron clustering could be detected, Fe can be used as probe for exploring the structure of the Opalinus clay sample. Unfortunately, Al and Mg (as octahedral cations) like Al and Si (as tetrahedral cations) cannot be discriminated by XAS, but further structural information on the clay sample can be derived using the chemical composition.

In clay minerals, Mg commonly fills octahedral sites. Assuming that the Mg content of 1:1 layers is low (e.g., Mermut and Cano, 2001), the number of Mg surrounding Fe in the 2:1 layers can be calculated. The sample contains 4.1 wt% Fe resulting in an average number of neighboring Fe atoms of 0.7 (Table 2). Considering 1.6 wt% Mg, the number of neighboring Mg becomes: (1.6 / 24.32) × 0.7 / (4.1 / 55.845) = 0.6. Consequently, the number of neighboring Al in the octahedral sheet is 3–0.7–0.6 = 1.7. Even though octahedral cations in dioctahedral 2:1 layers have three in-plane neighbors, structural formulae are written with only two octahedral cations yielding in this study a structural formula of the octahedral sheet of $[Al_{1.1}Mg_{0.4}Fe^{3+}{}_{0.5}]$. Furthermore, the sample contains low amounts of Na (0.7 wt%) and K (4.3 wt%), which can only be present as interlayer cations of 2:1 layers balancing the excess layer charge. Using similar methodology as above for Mg, the calculated stoichiometric coefficients of these cations are 0.2 and 0.7, respectively. The excess layer charge is thus 0.9, implying a net tetrahedral charge of 0.9–0.4 = 0.5 arising from Si^{4+} substitution by Al^{3+} (the net octahedral charge originating from Mg^{2+} substituting for trivalent cations is 0.4). The average chemical formula of the 2:1 layers of the sample can thus be written as $Na_{0.2}K_{0.7}(Al_{1.1}Mg_{0.4}Fe^{3+}{}_{0.5})(Si_{3.5}Al_{0.5})O_{10}(OH)_2$. The layer charge and K content are typical of illite (Meunier and Velde, 2004), the presence of interlayer Na may possibly be attributed to multiple washing with NaCl. The Fe content is moderate and makes 6.9 wt%. Consequently, the proportion of 2:1 lay-

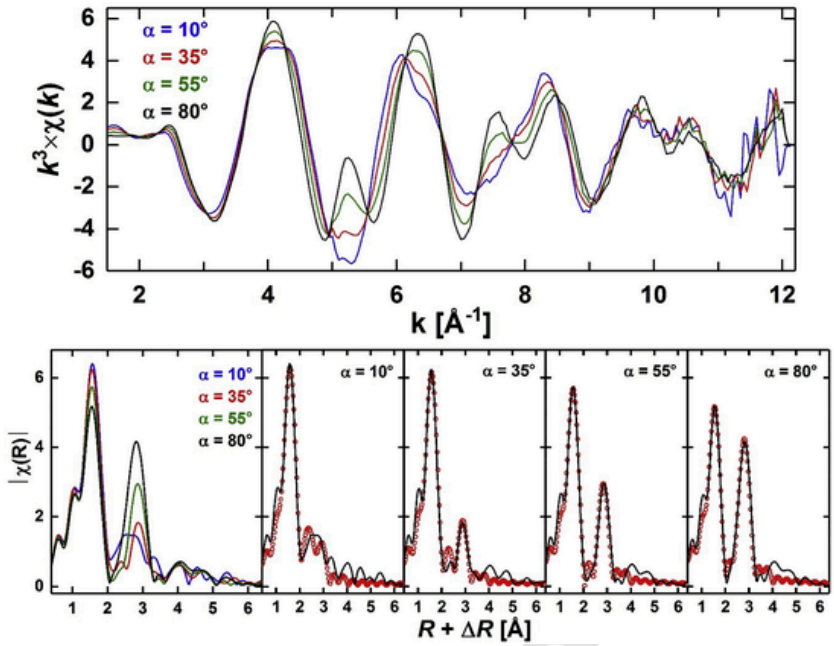

Fig. 4. Experimental polarized EXAFS spectra (up) and corresponding Fourier transforms (bottom left), and experimental (black line) and fits (red dots) to the Fourier transforms (bottom right) of the purified and fractioned Opalinus clay sample. Fit results are presented in Table 2. (For interpretation of the references to colour in this figure legend, the reader is referred to the web version of this article.)

Table 2
Results of fits to the polarized EXAFS data, uncertainties are indicated in parentheses otherwise parameters were fixed (data at all angles were fit simultaneously). Data are shown in Fig. 4.

Atomic shell	O	Al	Fe	Si
d [Å]	2.03(1)	3.03(1)	3.06	3.23
N^{10}	6.2(4)	2.8	0.9	1.6
N^{35}	6.0(4)	2.3	0.7	3.4
N^{55}	5.6(2)	1.6	0.5	6.4(7)
N^{80}	5.1	1.0(5)	0.3	8.9(10)
σ^2 [Å^2]	0.007	0.005	0.008	0.008

d is the interatomic distance, N is the coordination number at given angle indicated in superscript and σ^2 the mean squared displacement ("Debye-Waller" term). The shift in ionizing energy is $\Delta E_0 = 1.7(3)$ eV and the fit quality, representing the absolute misfit between theory and data, is $R_f = 0.013$.

ers in the investigated Opalinus clay sample amounts 4.1 / 0.069 = 59.42 wt%.

The structure of 2:1 layers was calculated assuming that it contains all Na, K, Fe and Mg of the purified and fractioned Opalinus clay sample, along with a fraction of Al and Si. The remaining fraction is thus made of compound(s) containing only Al and Si. Furthermore, these two elements represent 10.65 wt% and 24.27 wt%, respectively, of 2:1 layers and thus 6.33 wt% and 14.42 wt%, respectively, of the whole Opalinus clay sample. The remaining 40.58 wt% of minerals other than 2:1 layers in the whole clay sample thus contain 7.67 wt% Al and 9.68 wt% Si. Interestingly, XRPD evidenced the presence of significant amounts of the 1:1 layer kaolinite, which is made of only tetrahedral Si and octahedral Al. Since kaolinite ($Al_2Si_2O_5(OH)_4$) contains 20.90 wt% Al, the proportion of this phase in the Opalinus clay sample amounts 7.67 / 0.2090 = 36.70 wt%.

Calculations indicate that 2:1 and 1:1 layers represent 59.42 + 36.70 = 96.12 wt%, meaning that another compound makes 3.88 wt%. Actually, Si in these two structures represents 14.42 + 7.99 = 22.41 wt%, which is lower than the 24.1 wt% detected by SEM-EDX. The remaining 1.59 wt% Si can be attributed to admixed quartz which could not be unambiguously identified by XRPD because of its low amounts and because the most intense reflection of quartz at ~26.64° overlaps with the (006) plane of illite. Since Si represents 46.75 wt% of quartz, the proportion of this phase is 1.59 / 0.4675 = 3.40 wt%. Consequently, calculations show that the investigated Opalinus clay sample is made of 59.42 wt% of 2:1 layers, 36.70 wt% of 1:1 layer and 3.40 wt% quartz. The sum equals 59.42 + 36.70 + 3.40 = 99.52 wt% and deviations from the theoretical 100% are marginal. This finding supports the validity of the assumptions and calculations. Note that the ratio of 2:1 layers content to 1:1 layer content is reasonably close to reported values for the whole clay rock (Bath and Pearson, 2003).

4. Conclusion

The Opalinus clay rock was purified and the clay fraction separated. This clay fraction contains significant amounts of aluminum, substantial amounts of potassium and iron, and low amounts of magnesium. Sample analysis by XRPD and FTIR spectroscopy identified the presence of 1:1 and 2:1 layers clay minerals (e.g., kaolinite and illite (and possibly illite/smectite mixed layers)), with possible minutes amounts of quartz. Furthermore, infrared spectroscopy excludes Mg or Fe clustering and rather suggests the preferential formation of octahedral Mg-Fe pairs.

Polarized X-ray absorption spectroscopy at the Fe *K*-edge provided information on iron speciation. Pre-edge and EXAFS spectra evidenced the presence of sixfold coordinated ferric Fe only, the presence of ferrous ion or fourfold coordinated Fe in significant amounts is excluded. The number and orientation of neighboring cationic shells suggest a predominant Fe location within a dioctahedral octahedral sheet of 2:1 layers, and only marginal amounts within 1:1 layer. Combining results from XAS with that of chemical analysis allowed to calculate the chemical formula of the 2:1 layers, and further the proportions of 2:1 and 1:1 layers in the clay sample could be estimated.

Under (geo)chemical conditions expected to develop in deep geological repositories (e.g., microbial activity, evolution of hydrogen upon steel corrosion), octahedral Fe within clay minerals can possibly be reduced from trivalent to divalent oxidation state. Such modification in

oxidation state modifies the clay layer charge and causes an alteration of the reactivity of these minerals, thereby altering physicochemical properties of the clay rock. Such information can greatly help improving the accuracy and reliability of the safety case for such sites.

Credit Author Statement

NF designed the study, prepared and analyzed the sample, treated the data and wrote the article.

Uncited reference

Dyar et al., 2001

Declaration of Competing Interest

The author declares no competing financial interest.

Acknowledgements

The author thanks BGR (Hannover, Germany) for providing the Opalinus clay rock sample. The author acknowledges the ESRF (Grenoble, France) for provision of synchrotron radiation beam time and thanks I. Kieffer (CNRS, France) for assistance during measurements at the BM30B beamline. The author also thanks E. Soballa (KIT-INE, Germany) for SEM-EDX analysis.

References

ANDRA, 2005. Evaluation of the feasibility of a geological repository in an argillaceous formation. In: Dossier 2005, Argile. Chatenay-Malabry, France ISBN 2-916162-00-3.

Ankudinov, A L, Ravel, B, Rehr, J J, Conradson, S D, 1998. Real-space multiple-scattering calculation and interpretation of x-ray-absorption near-edge structure. Phys. Rev. B 58, 7565–7576.

A. Bath A. Gautschi Chapter 2. Geological settings and samples locations F.J. Pearson D. Arcos A. Bath J.-Y. Boisson A.M. Fernández H.-E. Gäbler ... H.N. Waber Mont Terri Project – Geochemistry of Water in the Opalinus Clay Formation at the Mont Terri Rock Laboratory 2003 Reports of the Federal Office for Water and Geology (FOWG), Geology Series No. 5. ISSN 1660-0754, ISBN 3-906723-59-3

A. Bath F.J. Pearson Chapter 3. Geochemical investigations F.J. Pearson D. Arcos A. Bath J.-Y. Boisson A.M. Fernández H.-E. Gäbler ... H.N. Waber Mont Terri Project – Geochemistry of Water in the Opalinus Clay Formation at the Mont Terri Rock Laboratory 2003 Reports of the Federal Office for Water and Geology (FOWG), Geology Series No. 5. ISSN 1660-0754, ISBN 3-906723-59-3

Berthonneau, J, Hoover, C G, Grauby, O, Baronnet, A, Pellenq, R J-M, Ulm, F-J, 2017. Crystal-chemistry control of the mechanical properties of 2:1 clay minerals. Applied Clay Sci. 143, 387–398.

Bishop, M E, Dong, H, Kukkadapu, R K, Liu, C, Edelmann, R E, 2011. Bioreduction of Fe-bearing clay minerals and their reactivity toward pertechnetate (Tc-99). Geochim. Cosmochim. Acta 75, 5229–5246.

Christidis, G E, Huff, W D, 2009. Geological aspects and genesis of bentonites. Elements 5, 93–98.

Cipriani, C, Mellini, M, Pratesi, G, Viti, C, 1997. Rodolicoite and Grattarolaite, two new phosphate minerals from Santa Barbara Mine, Italy. Eur. J. Mineral. 9, 1101–1106.

Dazas, B, Lanson, B, Delville, A, Robert, J-L, Komarneni, S, Michot, L J, Ferrage, E, 2015. Influence of tetrahedral layer charge on the organization of interlayer water and ions in synthetic Na-saturated smectites. J. Phys. Chem. C 119, 4158–4172.

Delaney, J S, Dyar, D M, Sutton, S R, 2001. Fe XANES spectra of iron-rich micas. Eur. J. Miner. 13, 1079–1098. doi:10.1127/0935-1221/2001/0013-1079.

Ewing, R C, Whittleston, R A, Yardley, B W D, 2016. Geological disposal of nuclear waste: a primer. Elements 12, 233–237.

Ferrage, E, Vidal, O, Mosser-Ruck, R, Cathelineau, M, Cuadros, J, 2011. A reinvestigation of smectite illitization in experimental hydrothermal conditions: results from X-ray diffraction and transmission electron microscopy. Am. Mineral. 96, 207–223.

Finck, N, Schlegel, M L, Bauer, A, 2015. Structural iron in dioctahedral and trioctahedral smectites: a polarized XAS study. Phys. Chem. Miner. 42, 847–859.

Finck, N, Bouby, M, Dardenne, K, Yokosawa, T, 2017. Yttrium co-precipitation with smectite: a polarized XAS and AsFlFFF study. Applied Clay Sci. 137, 11–21.

Finck, N, Schlegel, M L, Dardenne, K, Adam, C, Kraft, S, Bauer, A, Robert, J-L, 2019. Structural iron in smectites with different charge locations. Phys. Chem. Miner. 46, 639–661.

Gates, W P, 2008. Cation mass-valence sum (CM-VS) approach to assigning OH-bending bands in dioctahedral smectites. Clay Clay Miner. 56, 10–22.

Gorski, C A, Aeschbacher, M, Soltermann, D, Voegelin, A, Baeyens, B, Marques, Fernandes M, Hofstetter, T B, Sander, M, 2012. Redox properties of structural Fe in clay minerals. 1. Electrochemical quantification of electron-donating and –accepting capacities of smectites. Environ. Sci. Technol. 46, 9360–9368.

Gorski, C A, Klupfel, L E, Voegelin, A, Sander, M, Hofstetter, T B, 2013. Redox properties of structural Fe in clay minerals: 3. Relationships between smectite redox and structural properties. Environ. Sci. Technol. 47, 13477–13485.

Grambow, B, 2016. Geological disposal of radioactive waste in clay. Elements 12, 239–245.

Güven, N, 1988. Chapter 13. Smectites. In: Reviews in Mineralogy. In: Bailey, S W (Ed.), Vol. 19: Hydrous Phyllosilicates. Mineralogical Society of America, Washington DC ISBN13 978-0-939950-23-2.

Hahn, J E, Scott, R A, Hodgson, K O, Donach, S, Desjardins, S R, Solomon, E I, 1982. Observation of an electric quadrupole transition in the X-ray absorption spectrum of a Cu(II) complex. Chem. Phys. Lett. 88, 595–598.

Ilgen, A G, Kukkadapu, R K, Leung, K, Washington, R E, 2019. Swithing or iron in clay minerals. Environ. Sci. 6, 1704–1715.

Inoue, A, Watanabe, T, 1989. Infrared spectra of interstratified illite/smectite from hydrothermally altered tuffs (Shinzan, Japan) and diagenetic bentonites (Kinnekulle, Sweden). Clay Sci. 7, 263–275.

Joe-Wong, C, Brown, G E, Jr., Maher, K, 2017. Kinetics and products of chromium(VI) reduction by iron(II/III)-bearing clay minerals. Environ. Sci. Technol. 51, 9817–9825.

Kim, J, Dong, H, Seabaugh, J, Newell, S W, Eberl, D D, 2004. Role of microbes in the smectite-to-illite reaction. Science 303, 830–832.

Komadel, P, Madejová, J, Stucki, J W, 2006. Structural Fe(III) reduction in smectites. Appl. Clay Sci. 34, 88–94.

Lanson, B, Sakharov, B A, Claret, F, Drits, V A, 2009. Diagenetic smectite-to-illite transition in clay-rich sediments: a reappraisal of X-ray diffraction results using the multi-specimen method. Am. J. Sci. 309, 476–516.

Lantenois, S, Lanson, B, Muller, F, Bauer, A, Jullien, M, Plancon, A, 2005. Experimental study of smectite interaction with metal Fe at low temperature: 1. Smectite destabilization. Clays Clay Miner. 53, 597–612.

Li, G L, Zhou, C H, Fiore, S, Yu, W H, 2019. Interactions between microorganisms and clay minerals: New insights and broader applications. Appl. Clay Sci. 177, 91–113.

Liu, D, Dong, H, Bishop, M E, Zhang, J, Wang, H, Xie, S, Wang, S, Huang, L, Eberl, D D, 2012. Microbial reduction of structural iron in interstratified illite-smectite minerals by a sulfate reducing bacterium. Geobiology 10, 150–162.

Madejova, J, Komadel, P, 2001. Baseline studies of the clay minerals source clays: infrared methods. Clay Clay Miner. 49, 410–432.

Manceau, A, 1990. Distribution of cations among the octahedra of phyllosilicates - Insight from EXAFS. Can. Mineral. 28, 321–328.

Manceau, A, Schlegel, M L, 2001. Texture effects on polarized EXAFS amplitude. Phys. Chem. Miner. 28, 52–56.

Manceau, A, Chateigner, D, Gates, W P, 1998. Polarized EXAFS, distance-valence least-squares modeling (DVLS), and quantitative texture analysis approaches to the structural refinement of Garfield nontronite. Phys. Chem. Miner. 25, 347–365.

Manceau, A, Drits, V A, Lanson, B, Chateignier, D, Wu, J, Huo, D, Gates, W P, Stucki, J W, 2000. Oxidation-reduction mechanism of iron in dioctahedral smectites: II. Crystal chemistry of reduced Garfield nontronite. Am. Mineral. 85, 153–172.

Manceau, A, Lanson, B, Drits, V A, Chateigner, D, Gates, W P, Wu, J, Huo, D, Stucki, J W, 2000. Oxidation-reduction mechanism of iron in dioctahedral smectites: I. Crystal chemistry of oxidized reference nontronites. Am. Mineral. 85, 133–152.

Mermut, A R, Cano, A F, 2001. Baseline studies of the clay minerals society source clays: Chemical analyses of major elements. Clay Clay Miner. 49, 381–386.

Meunier, A, 2005. Clays. Springer, Berlin, Heidelberg.

Meunier, A, Velde, B, 1989. Solid solutions in I/S mixed-layer minerals and illite. Am. Mineral. 74, 1106–1112.

Meunier, A, Velde, B, 2004. Illite. In: Origins, Evolution and Metamorphism. Springer, Berlin.

Moore, D M, Reynolds, R C, Jr., 1997. X-Ray Diffraction and the Identification and Analysis of Clay Minerals. Second edition Oxford University Press, New York.

Mosser Ruck, R, Sterpenich, J, Michau, N, Jodin Caumon, M-C, Randi, A, Abdelmoula, M, Barres, O, Cathelineau, M, 2020. Serpentinization and H_2 production during an iron-clay interaction experiment at 90°C under low CO_2 pressure. Appl. Clay Sci. 191, 105609.

Mullican, C N, Yong, R N, Fukue, M, 2009. Some effects of microbial activity on the evolution of clay-based buffer properties in underground repositories. Appl. Clay Sci. 42, 331–335.

NAGRA, 2002. Project Opalinus Clay. Safety Report. Demonstration of disposal feasibility for spent fuel, vitrified high-level waste and long-lived intermediate-level waste (Entsorgungsnachweis). Technical Report 02-05, NAGRA, Wettingen, Switzerland.

NAGRA, 2002. Projekt Opalinuston. Synthese der geowissenschaftlichen Untersuchungsergebnisse. Entsorgungsnachweis für abgebrannte Brennelemente, verglaste hochradioaktive sowie langlebige mittelaktive Abfälle. Technischer Bericht 02-03, NAGRA, Wettingen, Switzerland.

Neumann, A, 2011. Redox properties of structural Fe in smectite clay minerals. ACS Symp. Ser. 1071, 361–379.

Neumann, A, Petit, S, Hofstetter, T B, 2011. Evaluation of redox-active iron sites in smectites using middle and near infrared spectroscopy. Geochim. Cosmochim. Acta 75, 2336–2355.

Nussbaum, C, Veuve, C, Bossart, P, 2008. Annex 3. Borehole Information System. In: Bossart, P, Thury, M (Eds.), Mont Terri Rock Laboratory. Project, Programme 1996 to 2007 and Results Rep. Swiss Geol. Surv. 3, ISSN 1661-9285, ISBN 978-3-302-40016-7.

Proux, O, Biquard, X, Lahera, E, Menthonnex, J-J, Prat, A, Ulrich, O, Soldo, Y, Trévisson, P, Kapoujvan, G, Perroux, G, Taunnier, P, Grand, D, Jeantet, P, Deleglise, M, Roux, J-P, Hazemann, J-L, 2005. FAME: a new beamline for X-ray absorption investigations of very dilute systems of environmental materials and biological interests. Phys. Scr. 115, 970–973.

Ravel, B, Newville, M, 2005. ATHENA, ARTEMIS, HEPHAESTUS: data analysis for X-ray absorption spectroscopy using IFEFFIT. J. Synchrotron Radiat. 12, 537–541.

Schlegel, M L, Manceau, A, 2013. Binding mechanism of Cu(II) at the clay-water interface by powder and polarized EXAFS spectroscopy. Geochim. Cosmochim. Acta 113, 113–124.

Schlegel, M L, Manceau, A, Chateigner, D, Charlet, L, 1999. Sorption of metal ions on clay minerals I. Polarized EXAFS evidence for the adsorption of Co on the edges of hectorite particles. J. Colloid Interface Sci. 215, 140–158.

Schlegel, M L, Bataillon, C, Brucker, F, Blanc, C, Prêt, D, Foy, E, Chorro, M, 2014. Corrosion of metal iron in contact with anoxic clay at 90°C: Characterization of the corrosion products after two years of interaction. Appl. Geochem. 51, 1–14.

Shannon, R D, 1976. Revised effective ionic radii and systematic study of interatomic distances in halides and chalcogenides. Acta Crystallogr. A 32, 751–767.

Stucki, J W, 2011. A review of the effects of iron redox cycles on smectite properties. C. R. Geosci. 343, 199–209.

Stucki, J W, Kostka, J E, 2006. Microbial reduction of iron in smectites. C. R. Geosci. 338, 468–475.

Stucki, J W, Golden, D C, Roth, C B, 1984. Preparation and handling of dithionite-reduced smectite suspensions. Clay Clay Miner. 32, 191–197.

Stucki, J W, Lee, K, Zhang, L, Larson, R A, 2002. Effects of iron oxidation state on the surface and structural properties of smectites. Pure Appl. Chem. 74, 2145–2158.

Tsipursky, S I, Drits, V A, 1984. The distribution of octahedral cations in the 2:1 layers of dioctahedal smectites studied by oblique-texture electron diffraction. Clay Miner. 19, 177–193.

Vantelon, D, Montarges-Pelletier, E, Michot, L J, Pelletier, M, Thomas, F, Briois, V, 2003. Iron distribution in the octahedral sheet of dioctahedral smectites. An Fe K-edge X-ray absorption spectroscopy study. Phys. Chem. Miner. 30, 44–53.

Vinci, D, Dazas, B, Ferrage, E, Lanson, M, Magnin, V, Findling, N, Lanson, B, 2020. Influence of layer charge on hydration properties of synthetic octahedrally-charged Na-saturated trioctahedral swelling phyllosilicates. Appl. Clay Sci. 184, 105404.

Waychunas, G A, Apted, M J, Brown, G E, 1983. X-ray K-edge absorption spectra of Fe minerals and model compounds. Phys. Chem. Miner. 10, 1–9.

Westre, T E, Kennepohl, P, DeWitt, J G, Hedman, B, Hodgson, K O, Solomon, E I, 1997. A multiplet analysis of Fe K-edge 1s → 3d pre-edge features of iron complexes. J. Am. Chem. Soc. 119, 6297–6314.

Xia, X, Idemitsu, K, Arima, T, Inagaki, Y, Ishidera, T, Kurosawa, S, Iijima, K, Sato, H, 2005. Corrosion of carbon steel in compacted bentonite and its effect on neptunium diffusion under reducing condition. Appl. Clay Sci. 28, 89–100.